10

Effect of tellurium impurity on structural and optical properties of ZnO ceramics

© A.K. Omaev, M.B. Ataev, M.E. Zobov

Amirkhanov Institute of Physics, Dagestan Scientific Center, Russian Academy of Sciences, Makhachkala, Russia

e-mail: omaev.67@mail.ru

Received March 18, 2024
Revised July 08, 2024
Accepted July 08, 2024

ZnO ceramic samples of different tellurium impurity are prepared by the uniaxial cold pressing method. The dependence of the optical and X-ray structural properties of zinc oxide ceramics on a tellurium concentration (0−9%) is examined. The annealing at 430 °C in ZnO:Te ceramics (9%) is shown to generate $ZnTeO_3$ phase, while annealing at 900 °C leads to the formation of Zn_3TeO_6 phase at Te content of 3, 7, 9%. Observations of the green luminescence spectrum of ceramics ZnO:Te (annealing at 430 °C) reveal that a tellurium doping of 1, 3% results in a shift of the spectrum to the long-wave region while at 7, 9% the spectrum returns to its original position. The annealing at 900 °C causes a substantial shift of the green luminescence spectrum (77 K) to the long-wave range. At 430 °C annealing, a violet luminescence band flares up, which goes out on annealing at 900 °C.

Keywords: Ceramics, photoluminescence, zinc oxide, structures.

DOI: 10.61011/EOS.2024.07.59651.6040-24

Introduction

In recent years, the interest in optical ceramics on the basis of both undoped and doped zinc oxide has grown dramatically. The increased attention to this material is attributed to the fact that zinc oxide is useful for creating optoelectronic devices and ionizing radiation detectors [1–3]. Developed reactive surface of ZnO makes it suitable for manufacturing sensing elements of gas detectors [4,5]. Depending on the method, defect composition and fabrication conditions, the ZnO spectrum (single-crystals, films, powders, ceramics) contains several radiation bands: exciton band near the absorption edge of the crystal (385−390 nm), violet (396−420 nm), medium blue (420−490 nm), green (500−590 nm), yellow-orange (590−640 nm) and red (700−770 nm) radiation bands [6,7].

There are various methods of fabricating optically sensitive ZnO-based materials. These are ZnO single-crystals, however, a lack of available high-quality single-crystal technologies constitutes a considerable constraint [8,9]. Transparent glass-ceramics based on nanocrystalline ZnO is another promising material. To activate the optical processes in ZnO-based glass-ceramic materials, the In, Ga, Co and rare earth element ions are used [10–12]. ZnO powder compression followed by annealing is another method of fabricating optical ceramics. Annealing may be performed both in vacuum and various gas media [1,3]. Impurity composition (Zn, In, Ga [13], Er and Yb [14]) has a considerable impact on the luminescent properties of ZnO-based ceramics. Also note that fabrication of ZnO-based optical ceramics is cheaper and easier than single-crystal growing [14].

There is currently very few studies investigating the effect of tellurium on the structure, morphology and optical properties of ZnO [15–20]. We have previously [21,22] demonstrated the possibility of tellurium doping of both oriented and polycrystalline ZnO films grown by the chemical transport reaction (CTR) method and identified the features of structure, morphology and photoluminescence (PL).

This paper sows the results of synthesis of Te-doped optically-active ZnO-based ceramics made by the uniaxial cold compaction method. Structure and luminescent properties of the ZnO:Te ceramics have been studies, the effect of the synthesis temperature and Te impurity concentrations on these properties has been investigated.

Experimental procedure

The study used the ZnO-based ceramics made by the uniaxial cold compaction [23] followed by annealing in air at 430 C and 900 °C during 20 h. UHP grade ZnO powder was used as feed stock for ceramics fabrication. To activate the optical processes in the ZnO-based ceramics, a Te impurity mechanically ground to fine-powder state was added to the original powder. Then the original ZnO powder was carefully stirred with the Te impurity, then compressed and annealed in air. Content of tellurium in the ZnO-based ceramics varied from 1 wt% to 9 wt%. The ZnO powder and its mixture with Te were compacted in the „Toroid“ high-pressure diamond anvil at 50 MPa. Disc-shaped ceramic samples 16 mm in diameter and 3 mm in thickness were made.

Shimadzu's XRD-7000 (Japan) diffractometer was used for X-ray examination of the samples. The prepared powder

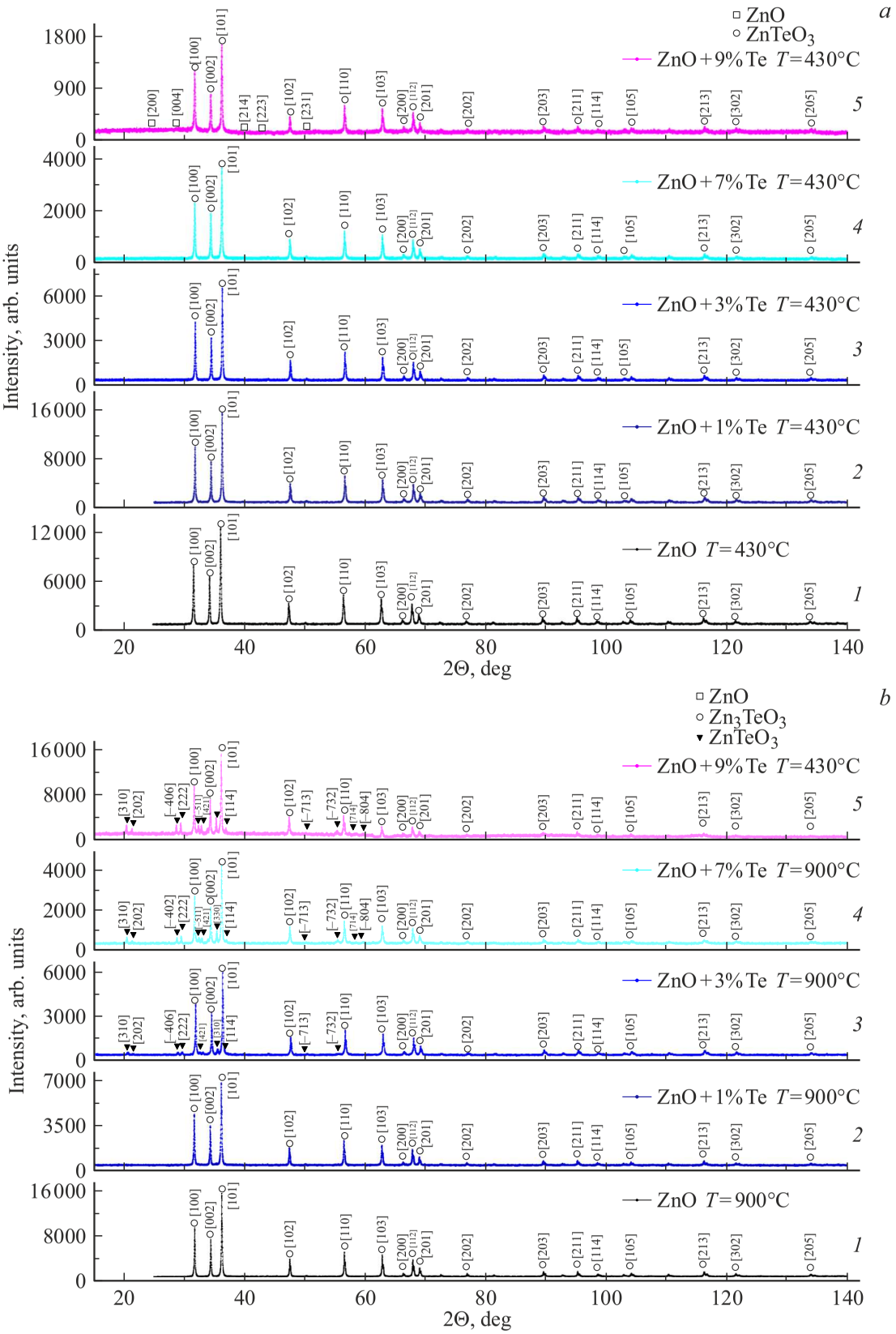

Figure 1. Diffraction pattern of the ZnO:Te (1–9%) ceramics, annealing at (*a*) 430 °C and (*b*) 900 °C: (*1*) 0% Te, (*2*) 1% Te, (*3*) 3% Te, (*4*) 7% Te, (*5*) 9% Te.

Updated lattice parameters and approximate content (C, wt%) of the identified phases

№	ZnO, P63mc		$ZnTeO_3$, pbca		Zn_3TeO_6, C2/c		Comment
	Lattice parameters	C, wt%	Lattice parameters	C, wt%	Lattice parameters	C, wt%	
1	$a = 3.2499$ Å $c = 5.2066$ Å	100	–	–	–	–	$x = 0\%$, $T = 430\,^\circ$C
2	$a = 3.2502$ Å $c = 5.2045$ Å	100	–	–	–	–	$x = 0\%$, $T = 900\,^\circ$C
3	$a = 3.2498$ Å $c = 5.2063$ Å	100	–	–	–	–	$x = 1\%$, $T = 430\,^\circ$C
4	$a = 3.2500$ Å $c = 5.2053$ Å	100	–	–	–	–	$x = 1\%$, $T = 900\,^\circ$C
5	$a = 3.2498$ Å $c = 5.2063$ Å	100	–	–	–	–	$x = 3\%$, $T = 430\,^\circ$C
6	$a = 3.2500$ Å $c = 5.2054$ Å	91	–	–	$a = 14.880$ Å $b = 8.8328$ Å $c = 10.3651$ Å $\beta = 92.985^\circ$	−9	$x = 3\%$, $T = 900^\circ$C
7	$a = 3.2500$ Å $c = 5.2054$ Å	100	–	–	–	–	$x = 7\%$, $T = 430\,^\circ$C
8	$a = 3.2498$ Å $c = 5, 2051$ Å	81	–	–	$a = 14.8861$ Å $b = 8.8308$ Å $c = 10.3584$ Å $\beta = 92.965^\circ$	19	$x = 7\%$, $T = 900\,^\circ$C
9	$a = 3.2498$ Å $c = 5.2059$ Å	96	$a = 6.3850$ Å $b = 12.261$ Å $c = 7.3552$ Å	4	–	–	$x = 9\%$, $T = 430\,^\circ$C
10	$a = 3.2497$ Å $c = 5.2051$ Å	73	–	–	$a = 14.8844$ Å $b = 8.8311$ Å $c = 10.3580$ Å $\beta = 92.967^\circ$	27	$x = 9\%$, $T = 900\,^\circ$C

sample was placed in the sample rotation module and recording was performed: beam focusing arrangement — the standard Bragg-Brentano geometry, CuK_α radiation wavelength 1.5406 Å using the Niβ-filter. The recorded diffraction patterns were pre-processed using software supplied with the diffractometer. Particular phases were sought in the samples using the ICDD (International Centre for Diffraction Data) PDF-4+ (Powder Diffraction File) database that contains more than 350 000 articles.

X-ray diffraction analysis of the ceramics composition identified the following phases: major ZnO, $ZnTeO_3$ and Zn_3TeO_6. The table shows updated lattice parameters and approximate phase compositions for all ceramic samples, including an amorphous phase.

Figure 1 shows X-ray images of the ZnO:Te (0−9%) ceramic samples taken at 430 C and 900 °C, respectively.

X-ray examinations (Figure 1, *a*) showed that the ZnO:Te (0−7%) ceramics fabricated at the annealing temperature of 430 °C doesn't display a phase associated with Te, while the ZnO:Te (9%) ceramics has the $ZnTeO_3$ phase. Annealing of the ZnO:Te ceramics at 900 °C leads to formation of the Zn_3TeO_6 phase in the ceramics with the Te impurity concentration of 3−9%, Figure 1, *b*.

For the purpose of PL examination, the sample placed in a cryostat and secured to the cold piping was excited by the KLM-F360-40 UV laser light. Laser excitation wavelength is 360 nm, beam diameter is 0.942 mm, light beam divergence is 0.9 mrad. Sample radiation was focused on the entrance slit of the MDR-23 monochromator. The Hamamatsu H10721-20 PMT type photomultiplier (spectral sensitivity range of 230−920 nm) is used as a radiation detector, then the signal arrives to the control and recording

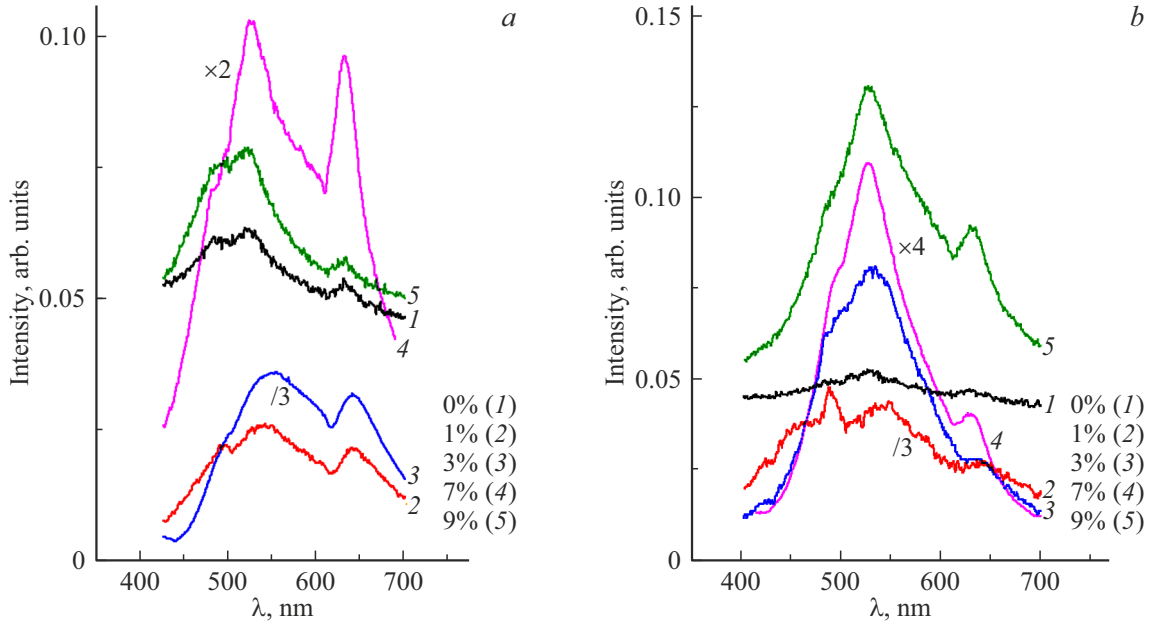

Figure 2. PL spectrum of the ZnO:Te (1−9%) ceramics, annealing at (*a*) 430 °C and (*b*) 900 °C: (*1*) 0% Te, (*2*) 1% Te, (*3*) 3% Te, (*4*) 7% Te, (*5*) 9% Te.

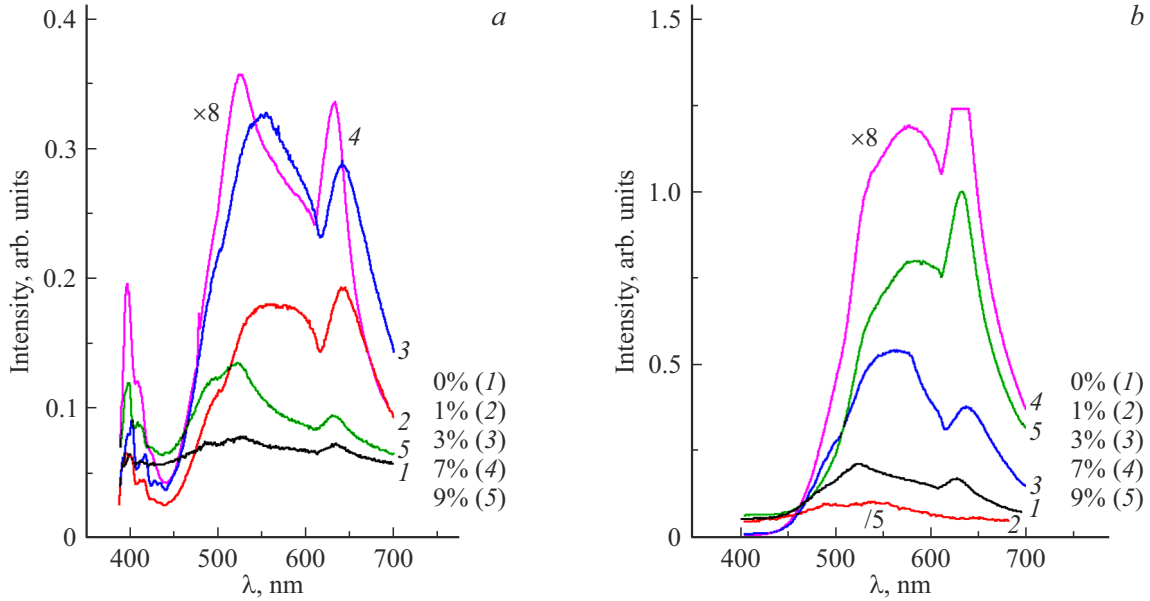

Figure 3. PL spectrum of the ZnO:Te (1−9%) ceramics, annealing at (*a*) 430 °C and (*b*) 900 °C: (*1*) 0% Te, (*2*) 1% Te, (*3*) 3% Te, (*4*) 7% Te, (*5*) 9% Te.

unit input. Computer-assisted unit control and experimental data processing are used.

Figure 2 shows the luminescence spectrum of the ZnO:Te (0−9%) ceramics measured at 300 K: (*a*) annealing at 430 °C and (*b*) annealing at 900 °C. Spectrum of the ZnO ceramics annealed at 430 °C and measured at 300 K contains the 490 nm, 520 nm and 630 nm lines, Figure 2, *a* (curve *1*). Doping with 1,3% Te, Figure 2, *a* (curves *2*, *3*) leads to a long-wavelength displacement of the green (550 nm) and yellow-orange (640 nm) portions of spectrum and to a decrease in the luminescence spectrum intensity by a factor of 2 to 4. When the concentration is increased up to 7, 9% Te in the ZnO-based ceramics, luminescence peaks are displaced into the initial positions and the intensity increases by a factor of 2 to 4. Note also that the Te impurity in the ZnO ceramics (annealing at 430 °C) doesn't affect the medium blue line (490 nm) position in the luminescence spectrum.

Figure 2, *b* shows the PL spectrum (300 K) of the ZnO-based ceramics fabricated at the annealing temperature of 900 °C. Initial spectrum of the undoped ZnO-based ceramics consists of the blue (490 nm), green (510, 525 nm) and yellow-orange (630 nm) lines, Figure 3, *b* (curve *1*). The 490 nm line, Figure 2, *b* (curve *2*), is poorly resolved in the initial spectrum with 1% Te doping, further increase in the Te percentage leads to its merging with the green region. Note also that 1, 3% Te doping leads to displacement of the green luminescence into the long-wavelength region (550, 530 nm), Figure 2, *b* (curves *2*, *3*). When the Te concentration is 7. 9%, the green luminescence peak returns into the initial position, Figure 2, *b* (curves *4*, *5*).

Visible luminescence spectra of the ZnO:Te (0–9%) ceramics (annealing at 430 °C) measured at 77 K are shown in Figure 3, *a*. The initial luminescence spectrum of the ZnO-based ceramics annealed at 430 °C is shown in Figure 3, *a* (curve *1*), and contains the 490 nm, 520 nm and 630 nm lines. Doping with 1, 3% Te, Figure 3, *a* (curves *2*, *3*) leads to a long-wavelength displacement of the 555 nm and 640 nm green and yellow-orange luminescence bands, respectively. Further increase in concentration (7, 9%) leads to displacement of the luminescence band peaks into their initial positions. A band at 490 nm displayed in the ZnO-based ceramics merges with the green band in case of Te (3, 7%) doping, Figure 3, *a* (curves *3*, *4*).

As the annealing temperature of the ZnO-based ceramics increases (900 °C), the luminescence spectrum peaks at 77 K consist of the 525 nm and 630 nm lines, Figure 3, *b* (curve *1*). Te doping (1, 3, 7, 9%) leads to the luminescence spectrum displacement at 77 K into a long-wavelength region: green (540 nm, 560 nm, 575 nm, 580 nm) and yellow-orange (645 nm, 637 nm, 630 nm, 632 nm), respectively, Figure 3, *b* (curve *2*, *3*, *4*, *5*). The medium blue (490 nm) band displayed in the ZnO:Te (1%) ceramics, Figure 3, *b* (curve *2*) merges with the green band as the Te concentration increases.

Note that Te doping of the ZnO ceramics (annealing at 430 °C) leads to violet luminescence band enhancement at 77 K. The initial violet luminescence spectrum is at 412 nm and 400 nm, Figure 3, *a* (curve *1*) due to charge carrier recombination in donor-acceptor pairs (DAP) [6]. Figure 3, *a* (curves *2*, *3*, *4*, *5*) shows that the violet band peak is displaced into a short-wavelength region. Increase in the Te concentration also leads to an increase in the violet light band intensity. When the Te concentration is 7%, the light intensity increases by an order of magnitude. Increase in the annealing temperature (up to 900 °C) of the ZnO:Te ceramics leads to violet luminescence quenching.

A wide visible light band is associated with the DAP recombination and various combinations, and with the presence of a residual impurity [1,6]. The main luminescence centers (490–560 nm) in ZnO are the Zn (V_{Zn}) and O (V_0) vacancies as well as interstitial Zn and O atoms [24]. Te doping of the ZnO-based ceramics and annealing at 430 °C lead to substitution of the O vacancies with Te and appearance of the $ZnTeO_3$ phase, and during annealing at 900 °C the interstitial Zn is substituted with Te and the Zn_3TeO_6 phase occurs, which is also supported in [16,25]. Such Te behavior in ZnO is associated with Te bipolarity in ZnO, i.e. when Zn is substituted - Te valence is 2, and when O vacancies are substituted — Te valence is +4 [15].

Conclusion

It follows from the foregoing that introduction of Te into the ZnO-based ceramics makes it possible to control both visible region and light intensity. It is shown that, depending on the annealing temperature, the $ZnTeO_3$ phase appears in he ZnO:Te ceramics (annealing at 430 °C), and after annealing at 900 °C - the Zn_3TeO_6 phase appears . Differences in the visible luminescence of the ceramics annealed at 430 C and 900 °C have been also identified. It is shown that introduction of Te into the ZnO-based ceramics considerably increases the visible luminescence band intensity. Increase in the annealing temperature leads to visible luminescence enhancement. Annealing of the ZnO:Te ceramics at 900 °C leads both to a significant displacement of the visible luminescence spectrum into a long-wavelength region and to quenching of the violet luminescence band (77 K). Te doping of the ZnO-based ceramics makes it possible to use it as a material for optoelectronic devices and high-sensitive gas detectors.

Acknowledgments

The authors are grateful to U.Z. Zalibekov, a research fellow, for his assistance in fabrication of the ceramics samples.

Conflict of interest

The authors declare that they have no conflict of interest.

References

[1] Ü. Özgür, Ya.I. Alivov, C. Liu, A. Teke, M.A. Reshchikov, S. Doğan, V. Avrutin, S.-J. Cho, H.Morkoç. J. Appl. Phys., **98**, 041301 (2005).
[2] Look David C. J. Electr. Mater., **35** (6), 1295–1305 (2006).
[3] E.I. Gorokhova, P.A. Rodnyi, K.A. Tchernenko, G.V. Anan'eva, S.B. Eron'ko, E.A. Oreshchenko, I.V. Khodyuk, E.P. Lokshin, G.B. Kunshina, O.G. Gromov, K.P. Lott. Opt. zhurnal, **78** (11), 85–95 (2011) (in Russian).
[4] L.A. Obvintseva. Ros. khim. zhurn., **LII** (2), 113–121 (2008) (in Russian).
[5] Chia-Yu Lin, Chii-Wann Lin, James J. Tunney, Kuo-Chuan Ho. Sensors and Actuators B., **146**, 28–34 (2010).
[6] I.P. Kuzmina, V.A. Nikitenko. *Okis zinka* (Nauka, M., 1984) (in Russian).
[7] P.A. Rodny, K.A. Chernenko, I.D. Venevtsev. Opt. i spektr., **125** (3), 357–363 (2018) (in Russian).
[8] F. Huang, Z. Lin, W. Lin et. al. Chin. Sci. Bull., **59** (12), 1235 (2014).

[9] A.E. Muslimov, V.M. Kanevsky, I.D. Venevtsev, A.M. Ismailov. Kristallografiya, **65** (5), 798–803 (2020) (in Russian).
[10] L.R. Pinckney. Phys. Chem. Glasses, **47** (2), 127–130 (2006).
[11] I.P. Alekseeva, O.S. Dymshits, A.A. Zhilin, S.S. Zapalova, D.V. Shemchuk. Opt. zhurnal, **81** (12), 27–33 (2014) (in Russian).
[12] B. Ghaemi, G. Zhao, S. Huang, J. Wang, J. Han. J. Am. Ceram. Soc., **95** (6), 1911–1914 (2012).
[13] M. Wang, L. Jiang, Y. Wang, E.J. Kim, S.H. Hahn. J. Am. Ceram. Soc., **98**. 3022–3028 (2015).
[14] O.S. Dymshits, E.I. Gorokhova, D.V. Shemchuk, I.P. Alekseeva, A.A. Khubetsov, P.A. Loiko, L.R. Basyrova, M.P. Shepilov, A.A. Zhilin, I.D. Venevtsev, S.B. Eron'ko, E.A. Oreshchenko. Sb. tr. Xll Mezhd. konf., pod red. S.A. Kozlova, 225–227 (2020) (in Russian).
[15] R. Suhu, K. Dileep, D.S. Negi, K.K. Nagaraja, R. Datta. Phys. Stat. Solidi B, **252** (8), 1743–1748 (2015).
[16] R. Suhu, K. Dileep, D.S. Negi, K.K. Nagaraja, C. Scheu, R. Datta. J. Cristal Growth., **410**, 69–76 (2015)
[17] S. Park, T. Minegishi1, D. Oh, D. Kim, J. Chang, T. Yao, T. Taishi, I. Yonenaga. Jpn. J. Appl. Phys., **52**, 055501 (2013).
[18] A. Iribarren, P. Fernandez, J. Piqueras. Phys. Status Solidi B, **251**, 3 (2013).
[19] F. Jamali-Sheini, R. Yousefi, M.R. Mahmoudian, N. AliBakr, A. Saaedi, N. Huang. Ceram. Int., **40**, 6 (2014).
[20] L. Porter, J.F. Muth, J. Narayan, J.V. Foreman, H.O. Everitt J. Appl. Phys., **100**, 123102 (2006).
[21] A.M. Bagamadova, A.Sh. Asvarov, A.K. Omaev, M.E. Zobov. Pisma v ZhTF, **44** (24), 52–58, (2018) (in Russian)
[22] A.K. Omaev, A.M. Bagamadova, M.E. Zobov. Opt. i spectr., **130** (3), 417–419 (2022) (in Russian).
[23] R.Ya. Popil'sky, Yu.E. Pivinsky. *Pressovanie poroshkovykh keramicheskikh mass* (M., Metallurgiya, 1983) (in Russian).
[24] S. Vempati, J. Mitra, P. Davson. Nanoscale Research Letters, **7**, 470, (2012).
[25] L. Cabral, V. Lopez-Richard, J.L.F. Da Silva, G.E. Marques, M.P. Lima, Y.J. Onofre, M.D. Teodoro, M.P.F. de Godoy. J. Lumin., **227**, 2–28 (2020).

Translated by E.Ilinskaya